JOURNAL OF MATERIALS SCIENCE **36** (2001) 3239–3246

# The influence of Poisson contraction on matrix cracking stress in fiber reinforced ceramics

YIH-CHERNG CHIANG
*Department of Mechanical Engineering, Chinese Culture University, No. 55, Hua-Kang Rd., Taipei, Taiwan*
*E-mail: ycchiang@staff.pccu.edu.tw*

The influence of Poisson contraction on the stresses for propagating a semi-infinite fiber-bridged crack in unidirectional fiber reinforced ceramics is studied in this paper. The situation of bonded fibers that is subjected to compressive pressure due to thermal expansion mismatch between the fiber and the matrix is considered in the present analysis. The results show that the Poisson contraction has profound effects on the matrix cracking stress predictions in the ceramic matrix composites, especially for the composites with high coefficient of friction. The Poisson contraction effects can be evidenced by the comparison of the present analysis with the Aveston, Cooper and Kelly (ACK) model. The roles played by the interfacial properties of the interfacial bonding energy and the coefficient of friction on the stresses for matrix cracking are discussed. 

## 1. Introduction

The inherently brittle ceramics can be toughened with the reinforcements such as long fibers or short whiskers. In a properly fabricated ceramic matrix composite, the initial matrix crack should be arrested or deflected by the fiber/matrix interface. For the unidirectional long fiber reinforced ceramics that are loaded in fiber axial direction, the initial matrix crack may result in a fiber-bridged crack transverse to the fibers. Finally, the repeated fiber-bridged cracks may be produced at regular spacing throughout the specimen before the final failure of the composite. Apparently, the composites possessing such multiple-matrix cracking exhibit more ductility and toughness than the monolithic ceramics.

The phenomenon of matrix cracking in brittle matrix composites has been a research subject for long standing. For theoretical modeling, different approach methodologies were adopted for predicting the critical stress to propagate a fiber-bridged crack. They include the energy balance approach (Aveston, Cooper and Kelly (ACK) [1]; Aveston and Kelly [2]; Budiansky, Hutchinson and Evans (BHE) [3], Chiang [4]), the distributed spring model (Marshall, Cox and Evans [5]; McCartney [6], Chiang, Wang and Chou [7]) and the continuous distributions of dislocation loops model (Meda and Steif [8]), etc. In the analyses of Ref. [1–7], the simple shear lag models which neglected the Poisson's effects were adopted to evaluate the stress-strain fields of the fiber and the matrix. The predicted matrix cracking stresses are closely related to the frictional shear stress that is assumed as a material constant. However, from the experimental study by Singh [9], it was reported that there was little correlation between the matrix cracking stresses and the frictional shear stress. Therefore, the exact roles played by the frictional shear stress on matrix cracking need to be further explored.

During matrix cracking, the bridged fibers should carry the additional load that was originally carried by the matrix. As a result, the additional Poisson contraction on the bridged fibers imposes the tensile force on the fiber/matrix interface. For the composites that are originally subjected to compressive pressure on the fiber/matrix interface, the imposed tensile force causes a reduction in the compressive pressure. According to the Coulomb friction low, this will result in a decrease in the frictional shear stress that changes the load transfer between the fiber and the matrix. Thus, it is expected that the additional Poisson contraction on the bridged fibers will cast an influence on the matrix cracking behaviors.

The intent of this paper is to evaluate the influence of Poisson contraction on the stresses for propagating a semi-infinite fiber-bridged crack in the unidirectional fiber reinforced ceramics. After the fiber/matrix interface is debonded in the wake of a fiber bridged crack, it is subjected to frictional resistance that is assumed to follow a Coulomb friction law. A shear-lag model, which includes the Poisson's effects and the friction in the debonded region, is adopted to calculate the stress and strain fields in the fiber and the matrix. The interfacial debonding criterion used in the present analysis is based upon the fracture mechanics approach, by which the debonding length in the crack-wake can be obtained. Subsequently, by using the energy balance approach, the formulation of the steady-state matrix cracking stress for propagating of a semi-infinite fiber-bridged crack is derived. The results show that the Poisson contraction has profound influences on the matrix cracking stress predictions in the ceramic

matrix composites, especially for the composites with high coefficient of friction. As compared to the ACK results for the purely frictional interface, the present model predicts the small matrix cracking stresses and the discrepancy between two models enlarges as the frictional coefficient increases. The presence of the interfacial bonding energy will increase the matrix cracking stresses and the influence of Poisson contraction on the matrix cracking stress predictions is similar to the case of the purely frictional interface. Furthermore, the predicted matrix cracking stresses of the bonded interface are shown to be less sensitive to the coefficient of friction than those of the purely frictional interface.

## 2. Fiber-matrix stress analysis

A unidirectional fiber reinforced ceramic with fiber volume fraction $c_f$ loaded by a remote uniform stress $\sigma$ normal to a semi-infinite crack is shown in Fig. 1. Here, three regions are identified with respect to the fiber-bridged crack. In the *downstream region*, which is sufficiently behind the crack tip, the stress and strain fields are uniform and the debonding length becomes constant with respect to the crack plane. In the *transient region*, the stress and strain fields are complex on both sides of the crack tip. It may be readily stated that the debonding length is diminishing as the fiber is approached from the downstream side to the crack tip. The upstream region is sufficiently ahead of the crack tip so that the stress and strain fields are again uniform.

The Poisson contraction effects on the fiber debonding and pullout behaviors in brittle matrix composites have been analyzed by Geo, Mai and Cotterell [10] and Hutchinson and Jensen [11]. It was adopted in their analyses that the axial and radial stresses in the debonded region transverse to the fiber can be characterized by a Lamé formulation. It was verified by numerical analysis [11] that the approximation by a Lamé solution is valid if the interfacial shear stress is small compared to the fiber axial stress. Therefore, the approximation of stress and strain by a Lamé approach is also adopted in the present analysis and the Lamé formulation of this section closely follows the analysis of Geo *et al*. [10].

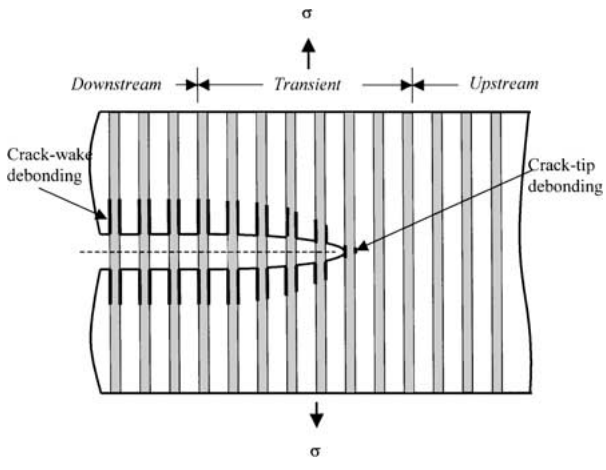


*Figure 1* Schematic representation of crack-tip and crack-wake debonding.

### 2.1. Downstream stresses

The free body diagram of the isolated composite cylinder model in the downstream region is illustrated in Fig. 2a, where the fiber closure traction that causes interfacial debonding between the fiber and matrix over the debonding length $l_d$. The radius of isolated composite cylinder $R$ is defined by

$$R = a/c_f^{1/2} \tag{1}$$

where $a$ is the fiber radius. The total axial stress in the *downstream region* satisfies

$$c_f\sigma_f(z) + c_m\sigma_m(z) = \sigma \tag{2}$$

where $\sigma_f(Z)$ and $\sigma_m(Z)$ denote the fiber and the matrix axial stresses, respectively.

Taking an arbitrary cross-section of the isolated composite cylinder (see Fig. 2b), we denote $\sigma_r$ and $\sigma_\theta$ as the

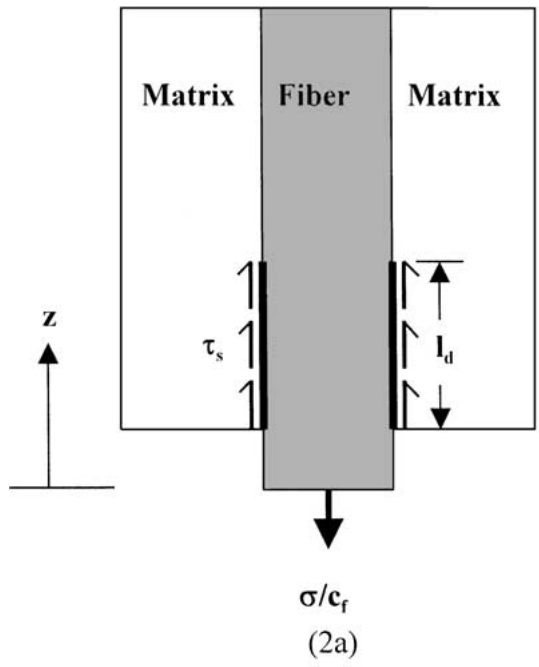


(2a)

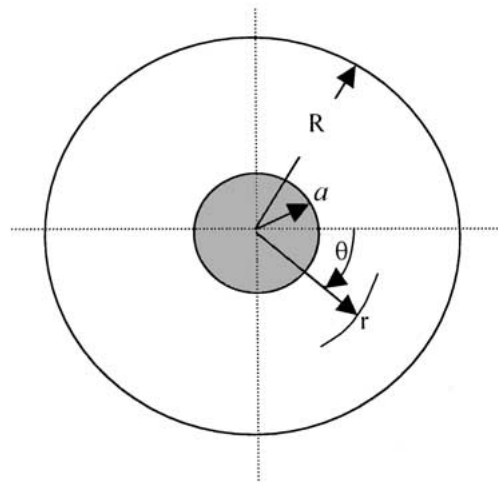


(2b)

*Figure 2* An isolated composite cylinder model.

radial and circumferential stresses. Under the assumption of isostrain in the fiber and matrix domains, the stress-strain relationships of the fiber and matrix are given by

$$\varepsilon_{\mathrm{f}} = (1/E_{\mathrm{f}})[\sigma_{\mathrm{f}}\nu_{\mathrm{f}} - (\sigma_{\mathrm{r}} + \sigma_{\theta})] \tag{3}$$

$$\varepsilon_{\mathrm{m}} = (1/E_{\mathrm{m}})[\sigma_{\mathrm{m}} - \nu_{\mathrm{m}}(\sigma_{\mathrm{r}} + \sigma_{\theta})] \tag{4}$$

where $\varepsilon$, $E$ and $\nu$ denote, respectively, the axial strain, Young's modulus and Poisson's ratio. The subscripts f and m indicate the fiber and matrix, respectively.

The boundary conditions of the isolated composite-cylinder model depicted in Fig. 2b are

$$(\sigma_{\mathrm{r}})_{\mathrm{r}=R} = 0 \tag{5}$$

$$(\sigma_{\mathrm{r}})_{\mathrm{r}=a^-} = (\sigma_{\mathrm{r}})_{\mathrm{r}=a^+} \tag{6}$$

$$(u_{\mathrm{r}})_{\mathrm{r}=a^-} = (u_{\mathrm{r}})_{\mathrm{r}=a^+} \tag{7}$$

where $u$ indicates the displacement.

The radial stress $\sigma_{\mathrm{r}}$ and the circumferential stress $\sigma_{\theta}$ can be solved by the classical Lamé formulation [12] with the satisfaction of the boundary conditions given by Equations 5–7. Thus, the radial stress $\sigma_{\mathrm{r}}$ and the circumferential stress $\sigma_{\theta}$ in the fiber cylinder domain are given by

$$\sigma_{\mathrm{r}} = \sigma_{\theta} = \frac{a\nu_{\mathrm{f}}\sigma_{\mathrm{f}} - \nu_{\mathrm{m}}\sigma_{\mathrm{m}}}{1 + \nu_{\mathrm{m}} + 2\gamma + \alpha(1 - \nu_{\mathrm{f}})} = q_0 \tag{8}$$

where

$$\alpha = E_{\mathrm{m}}/E_{\mathrm{f}} \tag{9}$$

and

$$\gamma = c_{\mathrm{f}}/c_{\mathrm{m}} \tag{10}$$

Accordingly, the radial stress $\sigma_{\mathrm{r}}$ and the circumferential stress $\sigma_{\theta}$ in the matrix ring domain are obtained:

$$\sigma_{\mathrm{r}} = \frac{\gamma R^2 q_0}{r^2} - \gamma q_0 \tag{11}$$

$$\sigma_{\theta} = -\frac{\gamma R^2 q_0}{r^2} - \gamma q_0 \tag{12}$$

Then, the stress-strain relationships of Equations 3 and 4 become

$$\varepsilon_{\mathrm{f}} = (1/E_{\mathrm{f}})[\sigma_{\mathrm{f}} - 2\nu_{\mathrm{f}}q_0] \tag{13}$$

$$\varepsilon_{\mathrm{m}} = (1/E_{\mathrm{m}})[\sigma_{\mathrm{m}} + 2\nu_{\mathrm{m}}\gamma q_0] \tag{14}$$

In the length $z \geq l_{\mathrm{d}}$, where no debonding has yet occurred between the fiber and matrix, the fiber axial strain equals to the matrix axial strain. Solving Equations 13 and 14 and Equation 2, the axial stresses of fiber and matrix in the length $z \geq l_{\mathrm{d}}$ are given by

$$\sigma_{\mathrm{f}}^{D} = \frac{1 - 2\nu_{\mathrm{m}}\kappa}{c_{\mathrm{m}}[\alpha + \gamma - 2\kappa(\alpha\nu_{\mathrm{f}} + \gamma\nu_{\mathrm{m}})]}\sigma \tag{15}$$

$$\sigma_{\mathrm{m}}^{D} = \frac{1}{c_{\mathrm{m}}}\left[1 - \frac{\gamma(1 - 2\nu_{\mathrm{m}}\kappa)}{\alpha + \gamma - 2\kappa(\alpha\nu_{\mathrm{f}} + \gamma\nu_{\mathrm{m}})}\right]\sigma \tag{16}$$

where

$$\kappa = \frac{\alpha\nu_{\mathrm{f}} + \gamma\nu_{\mathrm{m}}}{1 + \nu_{\mathrm{m}} + 2\gamma + \alpha(1 - \nu_{\mathrm{f}})} \tag{17}$$

In the length $0 \leq z < l_{\mathrm{d}}$, the fiber/matrix interface is debonded and resisted by a frictional force. If the fiber/matrix interface is under compressive pressure, the frictional shear stress $\tau_{\mathrm{s}}$ can be assumed to follow a Coulomb friction law:

$$\tau_{\mathrm{s}} = \mu(q_{\mathrm{i}} - q_0) \tag{18}$$

where $\mu$ is the coefficient of friction; and $q_{\mathrm{i}}$ is the initial interface pressure that occurs during fabrication of the composite (e.g. different thermal expansion of fiber and matrix) and $q_0$ is the tensile force due to the additional Poisson contraction of the fiber that causes a reduction in compressive stress.

The force equilibrium equation for a differential length of fiber in the debonded region is given by

$$\frac{d\sigma_{\mathrm{f}}}{dz} = -(2/a)\tau_{\mathrm{s}} \tag{19}$$

The boundary conditions at the crack plane $z = 0$ are

$$\sigma_{\mathrm{f}}(0) = \frac{\sigma}{c_{\mathrm{f}}} \tag{20}$$

$$\sigma_{\mathrm{m}}(0) = 0 \tag{21}$$

Solving Equations 2, 8, 18 and 19 with the boundary conditions given by Equations 20 and 21, the axial stresses of the fiber and the matrix and the frictional shear stress in the debonding length are given by

$$\sigma_{\mathrm{f}}^{D} = \frac{\sigma}{c_{\mathrm{f}}} - \frac{\alpha\nu_{\mathrm{f}}}{c_{\mathrm{f}}(\alpha\nu_{\mathrm{f}} + \gamma\nu_{\mathrm{m}})}(\bar{\sigma} - \sigma)(e^{\lambda z} - 1) \tag{22}$$

$$\sigma_{\mathrm{m}}^{D} = \frac{\alpha\nu_{\mathrm{f}}}{c_{\mathrm{m}}(\alpha\nu_{\mathrm{f}} + \gamma\nu_{\mathrm{m}})}(\bar{\sigma} - \sigma)(e^{\lambda z} - 1) \tag{23}$$

$$\tau_{\mathrm{s}}^{D} = \frac{a\alpha\nu_{\mathrm{f}}\lambda}{2c_{\mathrm{f}}(\alpha\nu_{\mathrm{f}} + \gamma\nu_{\mathrm{m}})}(\bar{\sigma} - \sigma)e^{\lambda z} \tag{24}$$

where

$$\lambda = 2\mu\kappa/a \tag{25}$$

and

$$\bar{\sigma} = \frac{c_{\mathrm{f}}q_{\mathrm{i}}}{\alpha\nu_{\mathrm{f}}}[1 + \nu_{\mathrm{m}} + 2\gamma + \alpha(1 - \nu_{\mathrm{f}})] \tag{26}$$

Let $w_{\mathrm{f}}(z)$ and $w_{\mathrm{m}}(z)$ denote the fiber and matrix axial displacements measured from the boundary $z = \infty$ and set $w_{\mathrm{f}}(\infty) = w_{\mathrm{m}}(\infty) = 0$. From Equations 13 and 14, the stress-strain relationships of the fiber and matrix can be expressed as

$$\varepsilon_{\mathrm{f}} = \frac{\mathrm{d}w_{\mathrm{f}}}{\mathrm{d}z} = \frac{1}{E_{\mathrm{f}}}[(1 - \nu_{\mathrm{f}}\kappa)\sigma_{\mathrm{f}} + \kappa_0\sigma] \tag{27}$$

$$\varepsilon_{\mathrm{m}} = \frac{\mathrm{d}w_{\mathrm{m}}}{\mathrm{d}z} = \frac{1}{E_{\mathrm{m}}}[(1 - \nu_{\mathrm{m}}\kappa)\sigma_{\mathrm{m}} + \alpha\kappa_o\sigma] \tag{28}$$

where

$$\kappa_0 = \frac{2\nu_f\nu_m}{c_m[1+\nu_m+2\gamma+\alpha(1-\nu_f)]} \tag{29}$$

Substituting Equations 15 and 16 and 22 and 23 into Eqs. (27-28), the axial displacements of the fiber and matrix in the debonding length, $0 \le z < l_d$, are obtained by integrating Equations 27 and 28: (for $L \to \infty$)

$$w_f(z) = -\frac{1-2\nu_f\kappa}{E_f}\left\{\frac{\sigma}{c_f}(l_d - z) - \frac{\alpha\nu_f(\bar{\sigma}-\sigma)}{c_f(\alpha\nu_f+\gamma\nu_m)}\left[\frac{e^{\lambda l_d}-e^{\lambda z}}{\lambda} - (l_d - z)\right] + \frac{(1-2\nu_m\kappa)(L-l_d)\sigma}{c_m[\alpha+\gamma-2\kappa(\alpha\nu_f+\gamma\nu_m)]}\right\} - \frac{\kappa_0(L-z)\sigma}{E_f} \tag{30}$$

$$w_m(z) = -\frac{1-2\nu_m\kappa}{E_m} \times\left\{\frac{\alpha\nu_f(\bar{\sigma}-\sigma)}{c_m(\alpha\nu_f+\gamma\nu_m)}\left[\frac{e^{\lambda l_d}-e^{\lambda z}}{\lambda} - (l_d - z)\right] + \frac{\alpha(1-2\nu_f\kappa)(L-l_d)\sigma}{c_m[\alpha+\gamma-2\kappa(\alpha\nu_f+\gamma\nu_m)]}\right\} - \frac{\kappa_0(L-z)\sigma}{E_f} \tag{31}$$

Then, the relative axial displacement $u(z)$ between the fiber and matrix in the debonding length, $0 \le z < l_d$, is obtained by

$$u(z) = |w_f(z) - w_m(z)| = -\alpha\nu_f(\bar{\sigma}-\sigma) \times\left[\frac{e^{\lambda l_d}-e^{\lambda z}}{\lambda} - (l_d - z)\right]\left[\frac{1-2\nu_m\kappa}{c_m E_m(\alpha\nu_f+\gamma\nu_m)} + \frac{1-2\nu_f\kappa}{c_f E_f(\alpha\nu_f+\gamma\nu_m)}\right] + \frac{1-2\nu_f\kappa}{c_f E_f}(l_d - z)\sigma \tag{32}$$

## 2.2. Upstream stresses

The *upstream region* (see Fig. 1) is so far away from the crack tip that the stress and strain fields are also uniform. Thus, the fiber and matrix have the same axial strains and the fiber and matrix axial stresses are given by

$$\sigma_f^U = \frac{1-2\nu_m\kappa}{c_m[\alpha+\gamma-2\kappa(\alpha\nu_f+\gamma\nu_m)]}\sigma \tag{33}$$

$$\sigma_m^U = \frac{1}{c_m}\left[1 - \frac{\gamma(1-2\nu_m\kappa)}{\alpha+\gamma-2\kappa(\alpha\nu_f+\gamma\nu_m)}\right]\sigma \tag{34}$$

These stresses are the same as those of the bonded length in the downstream region, given by Equations 15 and 16.

## 3. Interfacial debonding criterion

There are two different approaches to the crack-wake debonding problem, namely, the shear stress approach and the fracture mechanics approach. The shear stress approach is based upon a maximum shear stress criterion in which interfacial debonding occurs as the shear stress in the fiber/matrix interface reaches the shear strength of interface. On the other hand, the fracture mechanics approach treats interfacial debonding as a particular crack propagation problem in which interfacial debonding occurs as the strain energy release rate of interface attains the interfacial debonding toughness. Following the arguments of Gao, Mai and Cotterell [10] and Stang and Shah [13] that the fracture mechanics approach is preferred to the shear stress approach for the interfacial debonding problem, the fracture mechanics approach is adopted in the present analysis.

A general case of a cracked body is schematically shown in Fig. 3, in which a volume $V$ is loaded by tractions $T$ and $\tau_s$ on the surfaces $S_T$ and $S_F$ with corresponding displacements $dw$ and $du$, respectively. As the crack grows dA along the fractional surface $S_F$, the fracture criterion is proposed by [10]

$$\zeta_d = \frac{\partial}{2\partial A}\int_{S_T} T\,dw\,ds - \frac{\partial}{2\partial A}\int_{S_F}\tau_S\,du\,ds \tag{35}$$

where $\zeta_d$ is the interfacial debonding toughness. For the interfacial debonding problem (see Fig. 2a), the debonding process can be regarded as the crack propagation along the fiber/matrix interface. Thus, we have $A = 2\pi a l_d$, $ds = 2\pi a\,dz$ and $T = \sigma/c_f$, which is the fiber stress at the crack plane. In Equation 35, $u(z)$ is given by Equation 32 and $\int_{S_T} dw = -w_f(0)$ is given by Equation 30. Then, the debonding criterion of Equation 35 becomes

$$\zeta_d = \frac{aT}{4}\frac{\partial w_f(0)}{\partial l_d} - \frac{1}{2}\int_0^{l_d}\tau_s\frac{\partial u(z)}{\partial l_d}\,dz \tag{36}$$

Taking the derivatives of $w_f(0)$ and $u(z)$ with respect to $l_d$, Equation 36 becomes

$$\left[\frac{\alpha\nu_f(1+\beta)(\bar{\sigma}-\sigma)}{\alpha\nu_f+\gamma\nu_m}(e^{\lambda l_d}-1) - \sigma\right]^2 = \frac{4c_f^2E_f(1+\beta)}{a(1-2\nu_f\kappa)}\zeta_d \tag{37}$$

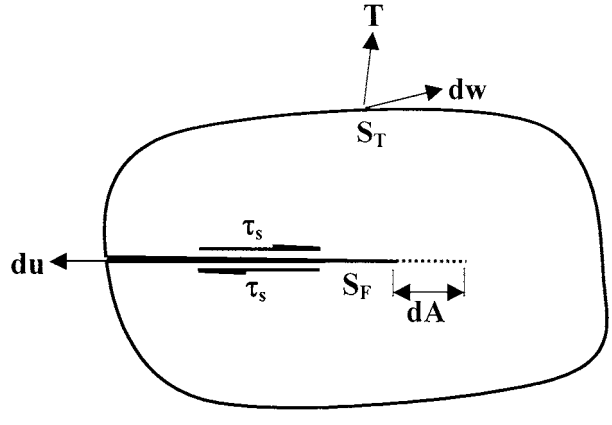


*Figure 3* Schematic showing of a general case of a crack body.

where

$$\beta = \frac{\gamma(1-2\nu_m\kappa)}{\alpha(1-2\nu_f\kappa)} \tag{38}$$

For the condition of frictionless interface in the debonding length (i.e., $\mu = 0$), the debonding stress $\sigma_0$ is given by Equation 37 with the substitution of $\lambda = 0$:

$$\sigma_0 = \left[\frac{4c_f^2 E_f(1+\beta)}{a(1-2\nu_f\kappa)}\zeta_d\right]^{1/2} \tag{39}$$

The debonding length $l_d$ can be obtained from Equation 37 and expressed as a function of $\sigma_0$:

$$l_d = \frac{\log\left[\dfrac{(\alpha\nu_f+\gamma\nu_m)(\sigma-\sigma_0)}{\alpha\nu_f(1+\beta)(\bar{\sigma}-\sigma)}+1\right]}{\lambda} \tag{40}$$

For the case of purely frictional interface (i.e., $\zeta_d = 0$), the debonding length $l_d$ reduces to the slipping length $l_s$ of unbonded composite:

$$l_s = \frac{\log\left[\dfrac{(\alpha\nu_f+\gamma\nu_m)\sigma}{\alpha\nu_f(1+\beta)(\bar{\sigma}-\sigma)}+1\right]}{\lambda} \tag{41}$$

## 4. Matrix cracking stress

The energy relationship to evaluate the steady-state matrix cracking stress for brittle matrix composites is expressed as (Refs. [3, 1])

$$\frac{1}{2}\int_{-\infty}^{\infty}\left[c_f\left(\sigma_f^U-\sigma_f^D\right)\left(\varepsilon_f^U-\varepsilon_f^D\right)+c_m\left(\sigma_m^U-\sigma_m^D\right)\times\left(\varepsilon_m^U-\varepsilon_m^D\right)\right]dz = c_m\zeta_m + 4c_f(l_d/a)\zeta_d \tag{42}$$

where $\zeta_m$ is the fracture toughness of matrix.

Substituting the strains of the fiber and matrix of Equations 27 and 28 into Equation 42, the formulation of steady-state matrix cracking stress becomes

$$\int_0^{l_d}\left[\frac{c_f(1-2\nu_f\kappa)}{E_f}\left(\sigma_f^U-\sigma_f^D\right)^2+\frac{c_m(1-2\nu_m\kappa)}{E_m}\times\left(\sigma_m^U-\sigma_m^D\right)^2\right]dz = c_m\zeta_m + 4c_f(l_d/a)\zeta_d \tag{43}$$

Further, substituting the downstream stresses of fiber and matrix given by Equations 22 and 23 and the upstream stresses of the fiber and matrix given by Equations 33 and 34 into Equation 43, the energy balance equation leads to the form of

$$\sigma^2 - \frac{2\phi(\psi_1+\phi\psi_2)\bar{\sigma}}{1+2\phi\psi_1+\phi^2\psi_2}\sigma + \frac{\phi\psi_2\bar{\sigma}^2-A}{1+2\phi\psi_1+\phi^2\psi_2} = 0 \tag{44}$$

where

$$\phi = \frac{\alpha\nu_f(1+\beta)}{\alpha\nu_f+\gamma\nu_m} \tag{45}$$

$$\psi_1 = \frac{e^{\lambda l_d}-1}{\lambda l_d} - 1 \tag{46}$$

$$\psi_2 = \frac{e^{2\lambda l_d}+3}{2\lambda l_d} - 2\frac{e^{\lambda l_d}}{\lambda l_d} + 1 \tag{47}$$

and

$$A = \frac{c_f c_m E_f E_m(1+\beta)^2}{c_f E_f(1-2\nu_f\kappa)+c_m E_m(1-2\nu_m\kappa)} \times\left(\frac{c_m\zeta_m}{l_d}+\frac{4c_f\zeta_d}{a}\right) \tag{48}$$

Substituting the debonding length $l_d$ of Equation 40 into Equation 44, the critical stress for matrix cracking $\sigma_{cr}$ can be solved by using the numerical root-finding method.

## 5. Results and discussion

The SiC/borosilicate composite is used for the case study and its material properties are listed in Table I.

The initial interface pressure $q_i$ that produced during fabrication is assumed mainly due to the difference of the thermal expansion between the fiber and matrix and it can be approximated by [3]

$$q_i = \frac{c_m E_m[1+\nu_f+(\nu_m-\nu_f)c_f E_f/E](\alpha_f-\alpha_m)\Delta T}{2\left\{1-(1-E/E_f)(1-\nu_f)/2+c_m(\nu_m-\nu_f)/2-(E/E_f)[\nu_f+(\nu_m-\nu_f)c_f E_f/E]^2\right\}} \tag{49}$$

where $\Delta T$ is the temperature change; and $\alpha_f$ and $\alpha_m$ are the linear thermal expansion coefficients over the range $\Delta T$.

TABLE I Properties of SiC/borosilicate composite

| | SiC(SCS-6 AVCO)/ borosilicate[#] |
|---|---|
| $E_f$ | 400 GPa |
| $E_m$ | 63 GPa |
| $\nu_f$ | 0.2 |
| $\nu_m$ | 0.3 |
| a | 70 $\mu$m |
| $\zeta_m$ | 8.92 J/m$^2$ |
| $\alpha_f$(radial) | $2.6\times10^{-6}$/°C |
| $\alpha_m$ | $3.2\times10^{-6}$/°C |
| $\Delta T$ | −500°C |

[#]Data from Ref. [14]

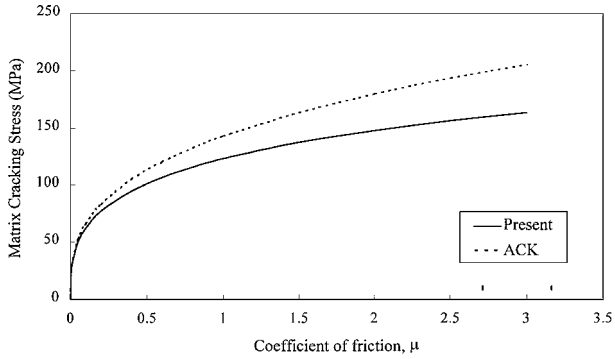


*Figure 4* Matrix cracking stress $\sigma_{cr}$ vs. coefficient of friction $\mu$ of unbonded interface for SiC/borosilicate at $c_f = 0.3$.

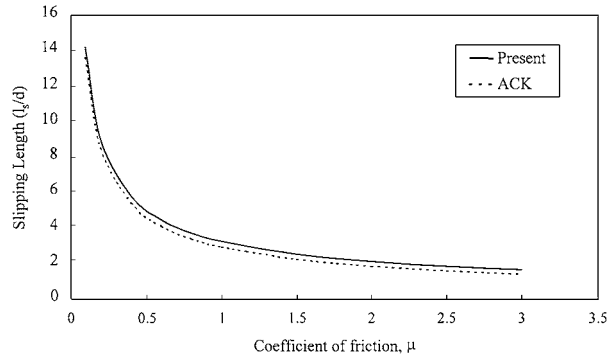


*Figure 5* Slipping length $l_s$ vs. coefficient of friction $\mu$ for SiC/borosilicate composite at $c_f = 0.3$, $d = 2a$.

For the unbonded fiber (i.e., $\zeta_d = 0$) but susceptible to frictional resistance in the slipping length, a well-known formulation of critical matrix cracking stress has been derived by ACK [1]:

$$\sigma_{cr} = \left( \frac{6 c_f E_f E \tau_s}{a c_m E_m^2} \zeta_m \right)^{1/3} \tag{50}$$

where $E$ is the composite axial modulus and approximated by rule-of-mixtures $E = c_f E_f + c_m E_m$. The ACK model neglects the effects of Poisson contraction such that the additional interfacial tensile stress $q_0$ could not be accounted for in their analysis. Therefore, the frictional shear stress $\tau_s$ given by Equation 18 reduces to $\mu q_i$ for the ACK model.

The Poisson contraction effects on the critical stresses for matrix cracking can be depicted in Fig. 4, where the critical matrix cracking stresses $\sigma_{cr}$ are plotted as a function of the coefficient of friction $\mu$ along with the ACK predictions. The difference of the $\sigma_{cr}$ predictions between two models illustrates the Poisson contraction effects on the matrix cracking stress predictions. As shown in Fig. 4, the difference of the $\sigma_{cr}$ predictions between two models enlarges as the frictional coefficient $\mu$ increases. This implies that the Poisson contraction has more profound influence on the matrix cracking stress for the composite with high frictional coefficient $\mu$. Fig. 5 plots the slipping lengths corresponding to the matrix cracking stresses of the present and ACK models depicted in Fig. 4. The present analysis predicts the longer slipping lengths than those of the ACK model. This phenomenon can be explained by the fact that the additional Poisson contraction of the fiber imposes a tensile force on the interface that causes a reduction in the interfacial compressive pressure and consequently results in the longer slipping lengths.

The influence of the relative matrix load carrying capability on the matrix cracking stresses is illustrated in Fig. 6, where the $\sigma_{cr}$ vs. $E_m/E_f$ at $E_f = 400$ Gpa and $\mu = 1$ is plotted along with the ACK prediction. The present and the ACK predictions show the same trend that $\sigma_{cr}$ decreases as the relative stiffness $E_m/E_f$ increases. Fig. 6 also indicates the discrepancy between two models enlarges as the relative stiffness $E_m/E_f$ decreases. It implies that the composite with smaller matrix stiffness has more profound Poisson contraction than the one with higher matrix stiffness.

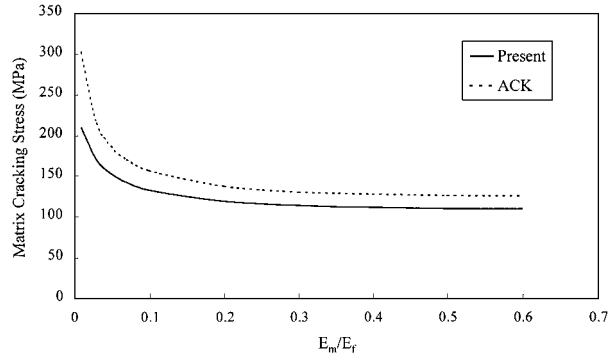


*Figure 6* Matrix cracking stresses vs. $E_m/E_f$ of unbonded interface for SiC/borosilicate at $E_f = 400$ Gpa and $\mu = 1$.

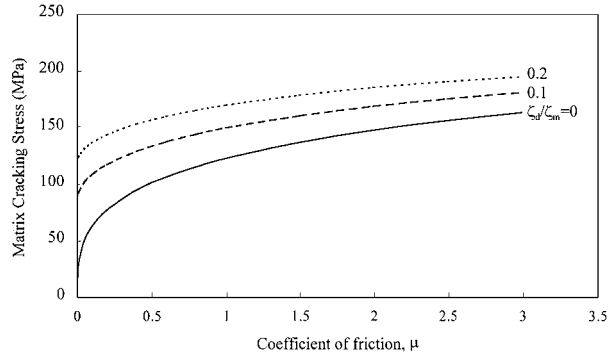


*Figure 7* Matrix cracking stress vs. coefficient of friction $\mu$ at different $\zeta_d/\zeta_m$ for SiC/borosilicate composite at $c_f = 0.3$.

The influences of interfacial debonding toughness and frictional shear stress on the matrix cracking stresses are illustrated in Fig. 7, in which the matrix cracking stresses are plotted as a function of frictional coefficient for different relative interfacial debonding toughnesses, $\zeta_d/\zeta_m$. Budiansky, Hutchinson and Evans [3] indicated that the interfacial debonding toughness $\zeta_d$ should be less than one-fifth of the matrix fracture toughness $\zeta_m$, otherwise the matrix crack tip fractures the fiber rather than deflects along the fiber/matrix interface. Therefore, the maximum relative interfacial debonding toughness, $\zeta_d/\zeta_m$, is chosen as 0.2 in the present analysis.

Similarly to the unbonded interface (i.e., $\zeta_d/\zeta_m = 0$), the matrix cracking stresses of the bonded interfaces of $\zeta_d/\zeta_m = 0.1$ and 0.2 increase as function of frictional coefficient, as depicted in Fig. 7. The presence of

interfacial bonding energy increases the matrix cracking stress. Moreover, the matrix cracking stress of the bonded interface becomes less sensitive to the frictional coefficient as compared to the unbonded interface. Singh [9] has experimentally studied the influence of frictional shear stress on the stress for matrix cracking by using fiber coating to obtain different frictional shear stress. Singh reported that there was little, if any, correlation between the frictional shear stress and the matrix cracking stress. In fact, the purely frictional interface is difficult to produce. Even the composite is slightly bonded, the matrix cracking stress will become less sensitive to the interfacial shear stress and the present analysis show the more close correlation with Singh's experimental observations. However, more experimental works are definitely needed to verify the relation between the matrix cracking stress and the frictional shear stress.

Fig. 8 illustrates the normalized $l_d$ vs. $\mu$ predictions for different relative interfacial debonding toughness, $\zeta_d/\zeta_m$. The debonding length is shown to decrease as $\zeta_d/\zeta_m$ and $\mu$ increase. However, the influence of $\zeta_d/\zeta_m$ and $\mu$ on the debonding length is diminished as $\zeta_d/\zeta_m$ and $\mu$ increase.

The results of the ACK model for purely frictional interface and the BHE model for the perfectly bonded interface are often quoted as the lower and upper bound for the matrix cracking stress predictions. In the present analysis, the matrix cracking stress corresponding to unbonded and frictionless interface (i.e., $\zeta_d = 0$ and $\mu \to 0$) can be considered as the lower bound prediction. On the other hand, the matrix cracking stress corresponding to the maximum interfacial debonding toughness (i.e., $\zeta_d/\zeta_m = 0.2$) with high frictional shear stress can be regarded as the upper bound prediction. The lower and upper bound predictions of matrix cracking stresses for SiC/borosilicate are illustrated in Fig. 9, where the ACK result with an assumed $\mu = 0.1$ and the BHE result are also plotted for comparison. It is noted that $\mu = 3$ represents a high frictional shear stress for SiC/borosilicate composite. It is shown in Fig. 9 that the unbonded interface with the small frictional coefficient can be well predicted by the ACK model and the perfectly bonded interface by the BHE model overestimates the upper bound matrix cracking stress predictions. Furthermore, the interface with the intermediate debonding toughness can be predicted by the present analysis.

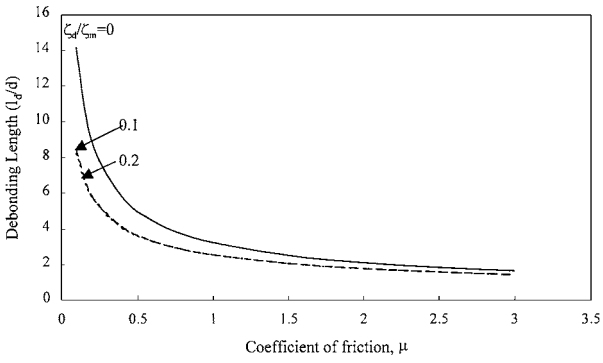


*Figure 8* Debonging length vs. coefficient of friction $\mu$ at different $\zeta_d/\zeta_m$ for SiC/borosilicate composite at $c_f = 0.3$.

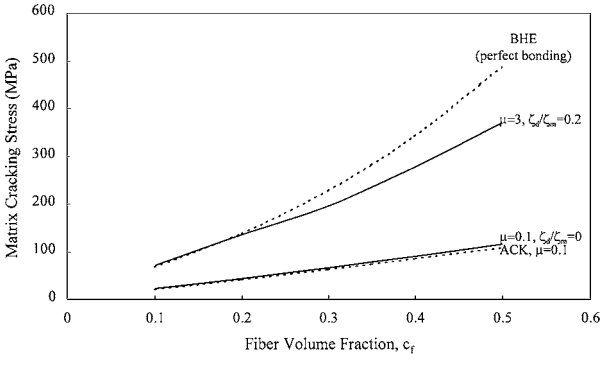


*Figure 9* The upper and lower bound predictions of matrix cracking stress for SiC/borosilicate composite.

## 6. Conclusions

1. In this paper, the effects of the Poisson contraction on matrix cracking stresses have been analyzed for unidirectional fiber reinforced ceramics. It has been shown that the Poisson contraction has profound influences on the matrix cracking stresses for ceramic matrix composites, especially for composites with high frictional coefficient.

2. At the on-set of matrix cracking, the fibers bridged the matrix crack should carry the additional load originally borne by the matrix. As a result, the additional Poisson contraction on the bridged fiber imposes a tensile force on the fiber/matrix interface that causes a reduction in compressive pressure (i.e., decrease frictional shear stress). Consequently, this results in the smaller matrix cracking stresses and longer slipping lengths, as depicted in Figs 4 and 5.

3. The interfacial debonding criterion used in the present analysis is based upon the fracture mechanics approach, by which the debonding length in the crack-wake can be obtained. Subsequently, by using the energy balance approach, the formulation of the steady-state matrix cracking stress can be derived and is given by Equation 44.

4. The presence of interfacial bonding energy increases the matrix cracking stress. Furthermore, the predicted matrix cracking stresses are shown to be less sensitive to the frictional coefficient as compared to the unbonded composite. This phenomenon was also observed by Singh [9].

## References


1. J. AVESTON, G. A. COOPER and A. KELLY, "Properties of Fiber Composites, Conference on Proceedings, National Physical Laboratory, IPC, England, 1971, p. 15.
2. J. AVESTON and A. KELLY, *J. Mater. Sci.* **8**(3) (1973) 352.
3. B. BUDIANSKY, J. W. HUTCHINSON and A. G. EVANS, *J. Mech. Phys. Solids* **34**(2) (1986) 167.
4. Y. C. CHIANG, *Engineering Fracture Mechanics* **65** (2000) 15.
5. D. B. MARSHALL, B. N. COX and A. G. EVANS, *Acta Metall.* **33**(11) (1985) 2013.
6. L. N. MCCARTNEY, *Proc. R. Soc.* **A409** (1987) 329.
7. Y. C. CHIANG, A. S. D. WANG and T. W. CHOU, *J. Mech. Phys. Solids* **41**(7) (1993) 1137.
8. G. MEDA and P. S. STEIF, *J. Mech. Phys. Solids* **42**(8) (1994) 1293.
9. R. N. SINGH, *J. Am. Ceram. Soc.* **73**(10) (1990) 2930.

10. Y. C. GAO, Y. W. MAI and B. COTTERELL, *J. of Applied Mathematics and Physics (ZAMP)*. **39**(7) (1988) 550.
11. J. W. HUTCHINSON and H. M. JENSEN, *Mechanics of Materials* **9** (1990) 139.
12. S. P. TIMOSHENKO and J. N. GOODER, "Theory of Elasticity," 3rd ed. (McGraw-Hill Book Co., Inc., New York, 1970).
13. H. STANG and S. P. SHAH, *J. Mat. Sci*. **21**(3) (1986) 953.
14. M. W. BARSOUM, P. KANGUTKAR and A. S. D. WANG, *Composite Science and Technology* **44** (1992) 257.

*Received 18 April 2000*
*and accepted 16 January 2001*